

# How alkaline compounds control atmospheric aerosol acidity

Vlassis A. Karydis<sup>1,2\*</sup>, Alexandra P. Tsimpidi<sup>1,2,3</sup>, Andrea Pozzer<sup>1,4</sup>, and Jos Lelieveld<sup>1,5</sup>

<sup>1</sup> Max Planck Institute for Chemistry, Atmospheric Chemistry Dept., Mainz, 55128, Germany.

<sup>2</sup> Forschungszentrum Jülich, Inst. for Energy and Climate Research, IEK-8, Jülich, 52425, Germany.

<sup>3</sup> National Observatory of Athens, Inst. for Environmental Research and Sustainable Development, Athens, 15236, Greece.

<sup>4</sup> International Centre for Theoretical Physics, Trieste, 34151, Italy

<sup>5</sup> The Cyprus Institute, Climate and Atmosphere Research Center Nicosia, 1645, Cyprus.

*Correspondence to:* Vlassis A. Karydis ([v.karydis@fz-juelich.de](mailto:v.karydis@fz-juelich.de))

**Abstract.** The acidity of atmospheric aerosols regulates the particulate mass, composition and toxicity, and has important consequences for public health, ecosystems and climate. Despite these broad impacts, the global distribution and evolution of aerosol acidity are unknown. We used the comprehensive atmospheric multiphase chemistry – climate model EMAC to investigate the main factors that control aerosol acidity and uncovered remarkable variability and unexpected trends during the past 50 years in different parts of the world. We find that alkaline compounds, notably ammonium, and to a lesser extent crustal cations, regulate the aerosol pH on a global scale. Given the importance of aerosols for the atmospheric energy budget, cloud formation, pollutant deposition and public health, alkaline species hold the key to control strategies for air quality and climate change.

## 1. Introduction

Aerosol acidity is a central property of atmospheric particulates that influence clouds, climate and air quality, including impacts on human health (Raizenne et al., 1996; Lelieveld et al., 2015). It affects the partitioning of semi-volatile acids between the gas and aerosol phases (Guo et al., 2016; Guo et al., 2017; Guo et al., 2018; Nenes et al., 2020), secondary organic aerosol (SOA) formation (Xu et al., 2015; Marais et al., 2016), the solubility of trace metals in aerosols (Oakes et al., 2012), associated with their toxicity (Fang et al., 2017) and nutrient capacity (Jickells et al., 2005), the activation of halogens that act as oxidants (Saiz-Lopez and von Glasow, 2012), the conversion of sulfur dioxide (Seinfeld and Pandis, 2006; Cheng et al., 2016), the particle hygroscopic growth and lifetime (Metzger et al., 2006; Abdelkader et al., 2015; Karydis et al., 2017), and atmospheric corrosivity (Leygraf et al., 2016). Direct measurement of aerosol acidity is difficult and associated with much uncertainty, being dependent on filter sampling and the H<sup>+</sup> molality in the aqueous extract, which is sensitive to artifacts (Pathak et al., 2004). Therefore, particle pH, a commonly used acidity metric of aqueous aerosols, is typically

30 inferred by proxy techniques (Hennigan et al., 2015;Pye et al., 2020). Two of the most common are the ion balance and the  
31 molar ratio methods. These methods do not consider the effects of aerosol water and multiphase interactions with gas phase  
32 species as well as the partial dissociation of acids (Hennigan et al., 2015). The simultaneous measurement of gas phase  
33 species can improve aerosol pH estimates by accounting for the phase partitioning of semi-volatile species (e.g.,  $\text{NH}_3$ ,  
34  $\text{HNO}_3$ ). However, the accuracy of this approach relies on the availability of information on these species in both the gas and  
35 aerosol phase, being scant in most cases.

36 The most reliable estimates of pH are obtained with thermodynamic equilibrium models, although the accuracy can be  
37 limited by not accounting for all ionic species. For example, most atmospheric chemistry models do not consider crustal  
38 elements (e.g.,  $\text{Ca}^{2+}$ ,  $\text{Mg}^{2+}$ ,  $\text{K}^+$ ) and  $\text{Na}^+$  in sea salt. These species affect the ion balance by influencing the phase partitioning  
39 of nitrate and ammonium, especially in areas where aeolian dust is abundant (Karydis et al., 2016). Here we present 50-year  
40 global acidity trends of fine aerosols (i.e. with a diameter  $< 2.5 \mu\text{m}$ ) by employing the EMAC chemistry – climate model  
41 (Jöckel et al., 2010). The pH calculations are performed online with the ISORROPIA II thermodynamic equilibrium model  
42 (Fountoukis and Nenes, 2007).

## 43 **2. Results and Discussion**

### 44 **2.1 Global variability of aerosol acidity**

45 Figure 1 shows the modeled near-surface distribution of fine aerosol acidity for the 2010-2015 period. We find  
46 predominantly acidic particles over the anthropogenically influenced regions in the northern hemisphere and the tropical  
47 biomass burning zones, and mostly alkaline particles over deserts and oceans, especially over the southern oceans. The pH  
48 typically ranges from 4.0 to 6.7 (5.3 on average) over the western USA since it is affected by crustal cations from the  
49 surrounding deserts. Polluted areas located downwind of crustal sources are of special interest since the pH calculations can  
50 be sensitive to the aerosol state assumption (see section 4.3). Over Pasadena, the base case model using the stable state mode  
51 estimates a mean pH of 5.9 units, while the sensitivity simulation with only liquid aerosols results in 2.7 pH units (equal to  
52 Guo et al. (2017) estimations by using the metastable assumption; Table S1). Our sensitivity analysis revealed that the  
53 aerosol state itself is not affected by the state assumption since both stable and metastable predict the same amount of water  
54 in the aerosol. Differences in the calculated pH can be due to the high concentrations of calcium from the Great Basin Desert  
55 which results in the precipitation of high amounts of  $\text{CaSO}_4$ , lowering the particle acidity (but without affecting the water  
56 activity since  $\text{CaSO}_4$  is insoluble and does not contribute to the MDRH depression). It is worth mentioning that calcium was  
57 not included in the Guo et al. (2017) study which helps explain the differences in the observed and simulated aerosol acidity.  
58 The simulated particle-phase fraction of nitrate over Pasadena is 40% using the stable state assumption and 32% using the  
59 metastable assumption, compared to the observationally derived 51%. Over Europe, the pH ranges from 2.6 to 6.7 (3.9 on  
60 average). Observational estimates of aerosol pH from the Po Valley (Squizzato et al., 2013;Masiol et al., 2020) and Cabauw

61 (Guo et al., 2018) support the relatively low acidity of fine aerosols over Europe (Table S1). Model calculations compare  
 62 well with observational estimates from Cabauw, however, result in higher pH (~1 unit) compared to values from Po Valley  
 63 (estimated by using the E-AIM model). Over East Asia the average pH is 4.7, ranging from 2.6 to 7.4. Relatively high pH are  
 64 found over regions where anthropogenic aerosols are mixed with aeolian dust, e.g., from the Gobi Desert, which decrease the  
 65 acidity (e.g., ~6 pH units over Hohhot, which agrees well with the estimations of Wang et al. (2019a)). The relatively low pH  
 66 in large parts of Asia is explained by strong SO<sub>2</sub> emissions and associated sulfate, which have increased strongly in the past  
 67 decades (e.g., over Guangzhou, supported by estimations of Jia et al. (2018)). Estimates of unrealistically high aerosol  
 68 acidity can result from omitting the gas phase concentrations of semi-volatile ions from the pH calculations (e.g., estimates  
 69 over Hong Kong (Yao et al., 2007; Xue et al., 2011), Singapore (Behera et al., 2013) and Shanghai (Pathak et al., 2009);  
 70 Table S1). At the same time, SO<sub>2</sub> emissions have decreased over Europe and USA, and recently in China. However, aerosols  
 71 over the eastern USA have remained acidic, with an average pH of 3.0 until recently, corroborating the findings of Weber et  
 72 al. (2016) and Lawal et al. (2018) that aerosol acidity over this region is less sensitive to SO<sub>2</sub> than to NH<sub>3</sub> emissions.  
 73 The aerosol pH over polluted northern hemispheric mid-latitudes (e.g., over East Asia) and the northern extratropical oceans  
 74 exhibits a clear seasonal pattern with lower values during boreal summer and higher ones during winter, driven by the  
 75 availability of ammonium and by the aerosol water content (Fig. 2). This is evident from both our model calculations and  
 76 from observational estimates mostly in heavily populated areas such as the Po Valley (Squizzato et al., 2013), Beijing (Tan  
 77 et al., 2018), and Tianjin (Shi et al., 2017), and to a lesser extent over areas strongly affected by aeolian dust (e.g., Hohhot;  
 78 Wang et al., 2019b) (Table S1). Over tropical regions, fine particulates have a pH between 3.2 and 7.4, being strongly  
 79 influenced by pyrogenic potassium, i.e., from widespread biomass burning (Metzger et al., 2006), and a high aerosol water  
 80 content. Observational estimates from Sao Paulo support these high pH values (Vieira-Filho et al., 2016), albeit with 1 unit  
 81 bias mainly related to the use of the E-AIM model. Over deserts, aerosols are relatively alkaline, with a pH up to 7.4.  
 82 Aerosols in the marine environment tend to be alkaline also, with a pH up to 7.4 over the southern oceans. Observational  
 83 estimates report highly acidic aerosols over the southern oceans due to the lack of gas phase input for the pH calculations  
 84 (Dall'Osto et al., 2019). Over the Arctic and the northern Atlantic and Pacific Oceans, aerosol acidity is significantly  
 85 enhanced by strong sulfur emissions from international shipping and pollution transport from industrialized areas (Fig. 1).  
 86 The pH over the northern extratropical oceans and the Arctic ranges from 2.0 to 7.0 with an average of about 5.2. The annual  
 87 cycle of aerosol acidity over these regions is strongly influenced by anthropogenic pollution, being relatively high during  
 88 boreal summer. Over the Antarctic, aerosol pH ranges from 4.5 to 7.0 and follows a clear seasonal pattern (Fig. 2).

## 89 **2.2 Temporal evolution of aerosol acidity**

90 Figure 1 and Table 1 present the aerosol pH over the period 1970-2020. We investigated the impacts of alkaline species by  
 91 omitting the emissions of ammonia and mineral cations in two sensitivity simulations.

## 92 2.2.1 Europe

93 Over Europe, the pH has increased strongly from about 2.8 during the 1970s to 3.9 recently. Especially during the 1990s  
94 NH<sub>3</sub> emissions over Europe increased significantly by 14%, while at the same time NO<sub>x</sub> and SO<sub>2</sub> emissions decreased by  
95 13% and 49%, respectively. While this trend has continued in the past decade, pH changes slowed because the sulfate and  
96 nitrate decreases have been compensated through volatilization of ammonia from the particles. In addition, the recently  
97 increasing cation/anion ratio is accompanied by a reduction of aerosol water, preventing a significant decrease of the aerosol  
98 acidity (Fig. S1). Overall, the increase of aerosol pH by more than 1 unit during the last 50 years had a significant impact on  
99 the gas-particle partitioning of semi-volatile acids, e.g., nitric acid, since their dissociation into ions enhances their solubility  
100 (Nah et al., 2018). Here, the fraction of nitrate in the particle phase relative to total nitrate (gas plus particle) has increased  
101 from ~70% to 85% (Fig. 3). The increase in aerosol pH has been accompanied by an increase in aerosol kappa  
102 hygroscopicity (Fig. 4). After the substantial reduction of SO<sub>2</sub> emissions, sulfate salts (e.g., ammonium sulfate with  
103 kappa=0.53) are replaced by more hygroscopic nitrate salts (e.g., ammonium nitrate with kappa=0.67) in the aerosol  
104 composition. In addition, the decrease of organic compound emissions during the last 50 years contributed to the increase of  
105 the aerosol hygroscopicity. Our sensitivity simulations reveal that aerosol acidity over Europe is highly sensitive to NH<sub>3</sub>  
106 emissions. Despite the decline of both SO<sub>2</sub> and NO<sub>x</sub> during the past decades, the aerosol would have remained highly acidic  
107 (pH ~1) in the absence of NH<sub>3</sub>.

## 108 2.2.2 North America

109 Over North America, aerosol acidity also decreased with SO<sub>2</sub> and NO<sub>x</sub> emissions. Nevertheless, these emissions are still  
110 relatively strong in the eastern USA (5 times higher than in the western USA) resulting in very acidic aerosols, with a pH  
111 ranging from 2.2 in 1971 to 3.3 recently (Figs. 1 and S1). Such acidic conditions promote the dissolution of metals (e.g., Fe,  
112 Mn, Cu) in ambient particles (Fang et al., 2017). Soluble transition metals in atmospheric aerosols have been linked to  
113 adverse health impacts since they generate reactive oxygen species, leading to oxidative stress and increased toxicity of fine  
114 particulate matter (Fang et al., 2017; Park et al., 2018). Since the solubility of transition metals increases exponentially below  
115 a pH of 3, the decrease of aerosol acidity over the eastern USA reported here suggests that the particles have become  
116 substantially less toxic in the past few decades. Similar to Europe, the increasing pH has resulted in a growing aerosol nitrate  
117 fraction from ~50% during the 1970s to 65% recently (Fig. 3), and to a strong increase of aerosol hygroscopicity by ~0.15  
118 units at the cloud base (Fig. 4). The role of NH<sub>3</sub> is critically important; without it the aerosol pH over the eastern USA would  
119 be close to zero. Over the western USA, the aerosol pH is higher (~5), being affected by aeolian dust from the Great Basin  
120 Desert, although NH<sub>3</sub> is still the most important alkaline buffer.

### 121 2.2.3 East and South Asia

122 In Asia, SO<sub>2</sub> and NO<sub>x</sub> emissions have increased drastically since 1970. However, the simultaneous increase of NH<sub>3</sub>  
123 emissions along with the presence of mineral dust from the surrounding deserts (i.e., Gobi, Taklimakan, Thar) decelerated  
124 the increase of aerosol acidity. Over East Asia, the aerosol pH decreased from about 5.3 during the 1970s to 4.5 in 2010.  
125 This change in aerosol acidity has affected the predominant pathway of sulfate formation through aerosol aqueous phase  
126 chemistry. Under acidic conditions, SO<sub>2</sub> is mainly oxidized by transition metal ions, while at pH > 5 the oxidation by O<sub>3</sub> and  
127 NO<sub>2</sub> predominates (Cheng et al., 2016). Therefore, the decrease of pH during the last 50 years, even though being relatively  
128 modest, was sufficient to turn-off sulfate production from O<sub>3</sub> oxidation (Fig. 5). At the same time, the increased aerosol  
129 acidity hinders the partitioning of nitric acid to the aerosol phase, reducing the aerosol nitrate fraction from 90% to 80% (Fig.  
130 3). Remarkably, the aerosol hygroscopicity has increased from ~0.3 in the 1970s to 0.45 recently (Fig. 4), revealing a reverse  
131 development compared to Europe and the USA. Here, the fraction of mineral dust in the aerosol is higher; therefore, the  
132 particles gained hygroscopicity by the acquired pollution solutes. Recently, the SO<sub>2</sub> emissions have dropped and the NO<sub>x</sub>  
133 emission increase has slowed in East Asia, while SO<sub>2</sub> emissions are soaring in South Asia. SO<sub>2</sub> emission trends since 2007  
134 have been so drastic that inventories and scenarios tend to overestimate the emitted SO<sub>2</sub>. Satellite observations indicate that  
135 India has recently overtaken China as the world largest emitter of SO<sub>2</sub> (Li et al., 2017). Following the satellite observations,  
136 we implemented the significant SO<sub>2</sub> reduction trends into our model (Fig. S2). Surprisingly, the effect only becomes  
137 noticeable over East Asia after 2016, when the aerosol pH started increasing by about 0.3 units, while we do not find any  
138 change over South Asia. This corroborates the strong buffering that we found over other regions such as Europe. Fig. 1  
139 shows that NH<sub>3</sub> has been the major buffer, supporting the recent findings of Zheng et al. (2020) that the acid-base pair of  
140 NH<sub>4</sub><sup>+</sup>/NH<sub>3</sub> provides the largest buffering capacity over East and South Asia. However, we also found that in East Asia and to  
141 a lesser extent in South Asia crustal elements, not considered in the study of Zheng et al. (2020), have contributed  
142 significantly on maintaining a mean pH of 4.5 – 5 in the past decade (Fig. 1). Calcium is the major crustal component of dust  
143 from the Gobi and Taklimakan deserts (Karydis et al., 2016) and unlike other crustal compounds it can react with sulfate  
144 ions and form insoluble CaSO<sub>4</sub>, which precipitates out of the aerosol aqueous phase. This interaction reduces the aqueous  
145 sulfate and thus the aerosol acidity.

### 146 2.2.4 Tropical forests, Middle East

147 Over tropical forests, aerosols are typically not very acidic with pH values >4. Note that organic acids were not included in  
148 the aerosol pH calculations, however, their contribution to the total ionic load is small (Andreae et al., 1988;Falkovich et al.,  
149 2005), and aerosol acidity can be attributed to inorganic acids. Over the Amazon and Congo basins, the aerosol pH remained  
150 around 5 since 1970. The Southeast Asian forest atmosphere is affected by pollution from mainland Asia, and the aerosol pH  
151 decreased to around 4 recently. This pH drop has enhanced SOA formation from isoprene, since under low-NO<sub>x</sub> conditions  
152 (typical over rainforests) the presence of acidifying sulfate increases the reactive uptake of epoxydiols (Xu et al.,

153 2015;Surratt et al., 2010). Nevertheless,  $\text{NH}_3$  emissions provide a remarkably strong buffer over all three tropical regions  
154 while mineral dust cations are also important over the Amazon and Congo forests. Further, the Middle East is affected by  
155 strong anthropogenic (fossil fuel related) and natural (aeolian dust) aerosol sources. Due to the high abundance of mineral  
156 dust, the pH has remained close to 7. Without crustal cations, the pH would drop to about 4. Despite the omnipresence of  
157 alkaline species from the surrounding deserts,  $\text{NH}_3$  still plays a central role in controlling the acidification of mineral dust  
158 aerosols, which can affect their hygroscopic growth and hence their climate forcing (Klingmuller et al., 2019;Klingmüller et  
159 al., 2020).

## 160 2.2.5 Oceans

161 Over the Arctic and northern extra-tropical oceans, aerosol acidity is strongly affected by pollution transport from the urban-  
162 industrial mid-latitudes. The Arctic aerosol pH is highly variable, remaining relatively low up to 1990 (~4.2), after which it  
163 increased to about 5.2. Crustal cations are found to play a significant role lowering the aerosol acidity. Over the northern  
164 extra-tropical oceans, aerosol pH has remained relatively constant (~4.8).  $\text{NH}_3$  provides an important alkaline buffer, and  
165 without it the aerosol pH would have been below 3.  $\text{NH}_3$  is also proved to be important over the tropical and southern extra-  
166 tropical oceans, where a noticeable increase in aerosol acidity occurred after June 1991, when the eruption of Mount  
167 Pinatubo in the Philippines released ~20 million tons of  $\text{SO}_2$  into the stratosphere (McCormick et al., 1995). The impact of  
168 Pinatubo sulfate, after returning to the troposphere, on aerosol acidity is mostly evident over Antarctica, where the pH  
169 dropped by 2 units, as the stratospheric circulation is strongest in the winter hemisphere. Over Antarctica concentrations of  
170 dust and especially of  $\text{NH}_3$  are very low, and Fig. 1 illustrates that only in this pristine environment the large Pinatubo  
171 anomaly could overwhelm the buffering by alkaline species. Except after Pinatubo, the pH has remained nearly constant at  
172 5.8 over Antarctica and about 5.5 in the tropics and 6.8 in the southern extra-tropics.

## 173 3. Conclusions

174 We find that aerosol pH is generally well-buffered by alkaline compounds, notably  $\text{NH}_3$  and in some areas crustal elements.  
175  $\text{NH}_3$  is found to supply remarkable buffering capacity on a global scale, from the polluted continents to the remote oceans. In  
176 the absence of  $\text{NH}_3$ , aerosols would be highly (to extremely) acidic in most of the world. Therefore, potential future changes  
177 in  $\text{NH}_3$  are critically important in this respect. Agriculture is the main  $\text{NH}_3$  source and a controlling factor in fine particle  
178 concentrations and health impacts in some areas (e.g., Europe) (Pozzer et al., 2017). The control of agricultural ammonia  
179 emissions must therefore be accompanied by very strong reductions of  $\text{SO}_2$  and  $\text{NO}_x$  to avoid that aerosols become highly  
180 acidic with implications for human health (aerosol toxicity), ecosystems (acid deposition and nutrient availability), clouds  
181 and climate (aerosol hygroscopicity).

## 182 4. Appendix A: Materials and Methods

### 183 4.1 Aerosol-chemistry-climate model

184 We used the ECHAM5/MESSy Atmospheric Chemistry (EMAC) model, which is a numerical chemistry and climate  
185 simulation system that describes lower and middle atmosphere processes (Jöckel et al., 2006). EMAC uses the Modular  
186 Earth Submodel System (MESSy2) (Jöckel et al., 2010) to link the different sub-models with an atmospheric dynamical core,  
187 being an updated version of the 5th generation European Centre - Hamburg general circulation model (ECHAM5) (Roeckner  
188 et al., 2006). EMAC has been extensively described and evaluated against in situ observations and satellite retrievals to  
189 compute particulate matter concentrations and composition, aerosol optical depth, acid deposition, gas phase mixing ratios,  
190 cloud properties, and meteorological parameters (Karydis et al., 2016; Pozzer et al., 2012; Tsimpidi et al., 2016; Karydis et al.,  
191 2017; Bacer et al., 2018). The spectral resolution of EMAC used in this study is T63L31, corresponding to a horizontal grid  
192 resolution of approximately  $1.9^\circ \times 1.9^\circ$  and 31 vertical layers extending up to 10 hPa (i.e., 25 km) from the surface. The  
193 presented model simulations encompass the 50-year period 1970-2020.

194 EMAC calculates fields of gas phase species online through the Module Efficiently Calculating the Chemistry of the  
195 Atmosphere (MECCA) Submodel (Sander et al., 2019). MECCA calculates the concentration of a range of gases, including  
196 aerosol precursor species (e.g.  $\text{SO}_2$ ,  $\text{NH}_3$ ,  $\text{NO}_x$ , DMS,  $\text{H}_2\text{SO}_4$  and DMSO) and the major oxidant species (e.g. OH,  $\text{H}_2\text{O}_2$ ,  
197  $\text{NO}_3$ , and  $\text{O}_3$ ). Aerosol microphysics are calculated by the Global Modal-aerosol eXtension (GMXe) module (Pringle et al.,  
198 2010). The organic aerosol formation and atmospheric evolution are calculated by the ORACLE Submodel (Tsimpidi et al.,  
199 2014, 2018). The aerosol size distribution is described by seven lognormal modes: four hydrophilic modes that cover the  
200 aerosol size spectrum of nucleation, Aitken, accumulation and coarse modes, and three hydrophobic modes that cover the  
201 same size range except nucleation. The aerosol composition within each size mode is uniform (internally mixed), however, it  
202 varies between modes (externally mixed). Each mode is defined in terms of total number concentration, number mean radius,  
203 and geometric standard deviation (Pringle et al., 2010). The removal of gas and aerosol species through wet and dry  
204 deposition is calculated within the SCAV (Tost et al., 2006) and DRYDEP (Kerkweg et al., 2006) submodels, respectively.  
205 The sedimentation of aerosols is calculated within the SEDI submodel (Kerkweg et al., 2006). The cloud cover,  
206 microphysics and precipitation of large scale clouds is calculated by the CLOUD Submodel (Roeckner et al., 2006) which  
207 uses a two-moment stratiform microphysical scheme (Lohmann and Ferrachat, 2010), and describes liquid droplet (Karydis  
208 et al., 2017) and ice crystal (Bacer et al., 2018) formation by accounting for the aerosol physicochemical properties. The  
209 effective hygroscopicity parameter  $\kappa$  is used to describe the influence of chemical composition on the cloud condensation  
210 nuclei (CCN) activity of atmospheric aerosols.  $\kappa$  is calculated using the mixing rule of Petters and Kreidenweis (Petters and  
211 Kreidenweis, 2007) and the individual  $\kappa$  parameter values for each inorganic salt (Petters and Kreidenweis, 2007; Sullivan et  
212 al., 2009). Organic aerosol species are assumed to have a constant hygroscopicity kappa parameter of 0.14 while bulk  
213 mineral dust and black carbon are assumed to have zero hygroscopicity.

## 214 4.2 Emissions

215 The vertically distributed (Pozzer et al., 2009) CMIP5 RCP8.5 emission inventory (van Vuuren et al., 2011) is used for the  
216 anthropogenic and biomass burning emissions during the years 1970-2020. Direct emissions of aerosol components from  
217 biofuel and open biomass burning are considered by using scaling factors applied on the emitted black carbon based on the  
218 findings of Akagi et al. (Akagi et al., 2011) (Table S2). Dust emission fluxes and emissions of crustal species ( $\text{Ca}^{2+}$ ,  $\text{Mg}^{2+}$ ,  
219  $\text{K}^+$ ,  $\text{Na}^+$ ) are calculated online as described by Klingmuller, et al. (Klingmuller et al., 2018) and based on the chemical  
220 composition of the emitted soil particles in every grid cell (Karydis et al., 2016); Table S3.  $\text{NO}_x$  produced by lightning is  
221 calculated online and distributed vertically based on the parameterization of Grewe, et al. (Grewe et al., 2001). The  
222 emissions of NO from soils are calculated online based on the algorithm of Yienger and Levy (Yienger and Levy, 1995). The  
223 oceanic DMS emissions are calculated online by the AIRSEA Submodel (Pozzer et al., 2006). The natural emissions of  $\text{NH}_3$   
224 are based on the GEIA database (Bouwman et al., 1997). Emissions of sea spray aerosols (assuming a composition suggested  
225 by Seinfeld and Pandis (Seinfeld and Pandis, 2006); Table S2) and volcanic degassing emissions of  $\text{SO}_2$  are based on the  
226 offline emission data set of AEROCOM (Dentener et al., 2006).

227

## 228 4.3 Thermodynamic model

229 The inorganic aerosol composition, which is of prime importance for the accurate pH calculation, is computed with the  
230 ISORROPIA-II thermodynamic equilibrium model (Fountoukis and Nenes, 2007). ISORROPIA-II calculates the  
231 gas/liquid/solid equilibrium partitioning of the  $\text{K}^+$ - $\text{Ca}^{2+}$ - $\text{Mg}^{2+}$ - $\text{NH}_4^+$ - $\text{Na}^+$ - $\text{SO}_4^{2-}$ - $\text{NO}_3^-$ - $\text{Cl}^-$ - $\text{H}_2\text{O}$  aerosol system and considers  
232 the presence of 15 aqueous phase components and 19 salts in the solid phase. ISORROPIA-II solves for the equilibrium state  
233 by considering the chemical potential of the species and minimizes the number of equations and iterations required by  
234 considering specific compositional “regimes”. The assumption of thermodynamic equilibrium is a good approximation for  
235 fine-mode aerosols that rapidly reach equilibrium. However, the equilibrium timescale for large particles is typically larger  
236 than the time step of the model (Meng and Seinfeld, 1996) leading to errors in the size distribution of semi-volatile ions like  
237 nitrate. Since the current study include reactions of nitric acid with coarse sea-salt and dust aerosol cations, the competition  
238 of fine and coarse particles for the available nitric acid can only be accurately represented by taking into account the kinetic  
239 limitations during condensation of  $\text{HNO}_3$  in the coarse mode aerosols. To account for kinetic limitations by mass transfer and  
240 transport between the gas and particle phases, the process of gas/aerosol partitioning is calculated in two stages (Pringle et  
241 al., 2010). First, the gaseous species that kinetically condense onto the aerosol phase within the model timestep are  
242 calculated assuming diffusion limited condensation (Vignati et al., 2004). Then, ISORROPIA-II re-distributes the mass  
243 between the gas and the aerosol phase assuming instant equilibrium between the two phases.

244 ISORROPIA-II is used in the forward mode, in which the total (i.e., gas and aerosol) concentrations are given as input.  
245 Reverse mode calculations (i.e. when only the aerosol phase composition is known) should be avoided since they are



sensitive to errors and infer bimodal behaviour with highly acidic or highly alkaline particles, depending on whether anions or cations are in excess (Song et al., 2018). While it is often assumed that aerosols are in a metastable state (i.e., composed only of a supersaturated aqueous phase), here we use ISORROPIA-II in the thermodynamically stable state mode where salts are allowed to precipitate once the aqueous phase becomes saturated. For this purpose, we have used the revised ISORROPIA-II model which includes modifications proposed by Song et al. (2018), who resolved coding errors related to pH calculations when the stable state assumption is used. By comparing with the benchmark thermodynamic model E-AIM, Song et al. (2018) found that ISORROPIA-II produces somewhat higher pH (by 0.1-0.7 units, negatively correlated with RH). However, E-AIM model versions either lack crustal cations from the ambient mixture of components (e.g. version II) (Clegg et al., 1998), or only include  $\text{Na}^+$  with the restriction that it should be used when  $\text{RH} > 60\%$  (e.g. version IV) (Friese and Ebel, 2010). Song et al. (2018) applied the revised ISORROPIA-II during winter haze events in eastern China and found that the assumed particle phase state, either stable or metastable, does not significantly impact the pH predictions.

We performed a sensitivity simulation with only liquid aerosols (i.e., metastable), which revealed that the assumed particle phase state does not significantly impact the pH calculations over oceans and polluted regions (e.g., Europe), however, the metastable assumption produces more acidic particles (up to 2 units of pH) in regions affected by high concentrations of crustal cations and consistently low RH values (Fig. S3). Fountoukis et al. (2007) have shown that the metastable solution predicts significant amounts of water below the mutual deliquescence relative humidity (MDRH, where all salts are simultaneously saturated with respect to all components). Further, the generally high calcium concentrations downwind of deserts results in increasing pH values due to the precipitation of insoluble salts such as the  $\text{CaSO}_4$ . The metastable state assumption fails to reproduce this since it treats only the ions in the aqueous phase. In general, high amounts of crustal species can significantly increase the aerosol pH which is consistent with the presence of excess carbonate in the aerosol phase (Meng et al., 1995). It is worth mentioning that the stable state solution algorithm of ISORROPIA II starts with assuming a dry aerosol, and based on the ambient RH dissolves each of the salts depending on their DRH. However, in the ambient atmosphere, when the RH over a wet particle is decreasing, the wet aerosol may not crystallize below the MDRH but instead remain in a metastable state affecting the uptake of water by the aerosol and thus the pH. This could be the case in some locations with high diurnal variations of RH. Our sensitivity calculations show that, overall, the stable state assumption produces an about 0.5 units higher global average pH than the metastable assumption. Karydis et al. (2016) have shown that while the aerosol state assumption has a marginal effect on the calculated nitrate aerosol tropospheric burden (2% change), it can be important over and downwind of deserts at very low RHs where nitrate is reduced by up to 60% by using the metastable assumption. This is in accord with the findings of Ansari and Pandis (2000) who suggested that the stable state results in higher concentrations of aerosol nitrate when the RH is low ( $< 35\%$ ) and/or sulfate to nitrate molar ratios are low ( $< 0.25$ ).

#### 277 4.4 pH calculations

278 The pH is defined as the negative decimal logarithm of the hydrogen ion activity ( $a_{H^+} = \gamma x_{H^+}$ ) in a solution:

279 
$$pH = -\log_{10}(\gamma x_{H^+}) \quad (A1)$$

280 where  $x_{H^+}$  is the molality of hydrogen ions in the solution and  $\gamma$  is the ion activity coefficient of hydrogen. Assuming that  $\gamma$   
281 is unity, the aerosol pH can be calculated by using the hydrogen ion concentration in the aqueous aerosol phase calculated by  
282 ISORROPIA-II (in mole m<sup>-3</sup>) and the aerosol water content calculated by GMXe (in mole Kg<sup>-1</sup>). GMXe assumes that particle  
283 modes are internally mixed and takes into account the contribution of both inorganic and organic (based on the organic  
284 hygroscopicity parameter, kappa=0.14 (Tsimpidi et al., 2014)) species to aerosol water.

285 The aerosol pH is calculated online at each timestep, and output stored every five hours based on instantaneous  
286 concentrations of fine aerosol water and hydrogen ions. The average pH values shown in the manuscript are based on the  
287 calculated instantaneous mean pH values. According to the Jensen's inequality (Jensen, 1906), the average of the  
288 instantaneous pH values is less than or equal to the pH calculated based on the average of the water and hydrogen ion  
289 instantaneous values. We estimate that the average pH calculated based on 5-hourly instantaneous values is approximately 1-  
290 3 (~2 globally averaged) units higher than the pH calculated based on the average water and hydrogen ion concentrations. By  
291 including online gas-particle partitioning calculations of the NH<sub>3</sub>/HNO<sub>3</sub> system in polluted air, as applied here, we find that  
292 the aerosol pH is higher by approximately one unit (Guo et al., 2015). Hence by neglecting these aspects the aerosol pH  
293 would be low-biased by about 3 units.

294

#### 295 4.5 Comparison against pH estimations from field derived PM<sub>2.5</sub> compositional data

296 The pH calculated here is compared against pH estimations from field derived PM<sub>2.5</sub> compositional data around the  
297 world compiled by Pye et al. (2020) (Table S1). pH data derived from other aerosol sizes (e.g., PM<sub>1</sub>) has been omitted since  
298 aerosol acidity can vary significantly with size (Zakoura et al., 2020). It should be emphasized that the comparison presented  
299 in Table S1 aims to corroborate the spatial variability of pH found in this study and not to evaluate the model calculations.  
300 Since direct measurements of aerosol acidity are not available, the observation-based aerosol pH is estimated by employing  
301 thermodynamic equilibrium models (e.g., ISORROPIA) and making assumptions that can significantly affect the results,  
302 especially when the data are averaged over extended periods, while RH conditions during data collection are not always  
303 accounted for, e.g. in studies based on filter sampling. The calculation of aerosol acidity on a global scale requires the  
304 advanced treatment of atmospheric aerosol chemical complexity, representing the real atmosphere, and beyond the  
305 conventional methods used by chemistry-climate models (CCM). The atmospheric chemistry model system EMAC is an  
306 ideal tool for this purpose since it is one of the most comprehensive CCM containing advanced descriptions of the aerosol

thermodynamics (including e.g. dust-pollution interactions) and organic aerosol formation and atmospheric aging (affecting the aerosol water). Our model calculations for aerosol acidity are based on some processes/factors that are not included explicitly, usually neglected by model calculations used to constrain the aerosol acidity from observations. Sources of discrepancy between the pH calculations can be the following:

- The stable/metastable assumption does not affect the pH most of the time, however, in some cases with low RHs and the presence of crustal cations, the metastable assumption results in lower pHs (see section 4.3).
- Crustal species from deserts and  $\text{Na}^+$  from sea salt can elevate the pH significantly in some locations, however, these are often neglected in observations.
- The organic aerosols (which are treated comprehensively by our model using the module ORACLE and the volatility basis set framework (Tsimpidi et al., 2014)) can contribute significantly to the aerosol water, and thus increase the aerosol pH. This contribution is not considered by many observational studies.
- Including gas phase species (e.g.,  $\text{NH}_3$ ,  $\text{HNO}_3$ ) in the pH calculations is important. Using only the aerosol-phase as input (i.e., reverse mode) the inferred pH exhibits bimodal behaviour with very acidic or alkaline values depending on whether anions or cations are in excess (Hennigan et al., 2015). Even if the forward mode is used (without gas phase input), the calculated aerosol pH is biased low (approximately 1 pH unit) due to the repartition of semi-volatile anions (i.e.,  $\text{NH}_3$ ) to the gas phase to establish equilibrium (Guo et al., 2015).
- Another important aspect, not explicitly mentioned in many studies, relates to the methods used to derive the campaign-average (or for 3D models the simulated average) pH. In our model the aerosol pH is calculated online (2-minute time resolution), while output is stored every five hours based on instantaneous concentrations of fine aerosol  $\text{H}_2\text{O}$  and  $\text{H}^+$ . This mimics 5-hourly aerosol sampling. Then, the average pH values are calculated from the instantaneous mean pH values (see section 4.4). Often models use average values (and not instantaneous) as output, or field-derived pH calculations use average observed  $\text{H}_2\text{O}$  and  $\text{H}^+$  values, which can result in important underestimation (by  $\sim 1$ -3 units) of the aerosol pH (Jensen, 1906).
- Some unrealistically high pH values in a few past studies resulted from coding errors in the stable state assumption of the ISORROPIA II model, which have been corrected in our study following the recommendation of Song et al. (2018).
- The type of thermodynamic model used is also important. Song et al. (2018) found that ISORROPIA-II produces somewhat higher pH (by 0.1-0.7 units, negatively correlated with RH) compared to the thermodynamic model E-AIM, which is used to observationally-constrain pH in some studies.
- Measurements of  $\text{PM}_{2.5}$  nitrate are not always reliable because of artifacts associated with the volatility of ammonium nitrate (Schaap et al., 2004). Ammonium and nitrate can partially evaporate from Teflon filters at temperatures between 15 to 20 °C and can evaporate completely at temperatures above. The evaporation from quartz filters is also significant at temperatures higher than 20 °C. This systematic underestimation of ammonium nitrate can affect the observed chemical composition of the aerosol and thus the pH calculations.

340 • The comparison between global model output and observations at specific locations. This also concerns the aerosol  
 341 concentrations but is especially important for the aerosol acidity. Apart from the size of the model grid cells (i.e., ~  
 342 1.9°x1.9°), the altitude is also important. The first vertical layer of EMAC is approximately 67m in height. On the other  
 343 hand, ground observations are typically collected in a height up to 3 m. While the aerosols within size modes simulated  
 344 in our model are well-mixed, perhaps this is not the case for the aerosols observed at the surface and potentially close to  
 345 sources, and thus the aerosol acidity may be higher (e.g., due to the higher contribution from local primary sources like  
 346 SO<sub>4</sub><sup>-2</sup>, lower water amounts in the aerosol, or lower concentrations of semi-volatile cations like NH<sub>4</sub><sup>+</sup>)  
 347

#### 348 4.6 Partitioning of nitric acid between the gas and aerosol phases

349 The impact of pH on the fraction of nitrate in the particle phase relative to total nitrate (gas plus particle), i.e.,  $\varepsilon(\text{NO}_3^-)$ ,  
 350 during the 50 years of simulation in specific regions is calculated as follows (Nah et al., 2018):

$$351 \quad \varepsilon(\text{NO}_3^-) = \frac{H_{\text{HNO}_3}^* \text{WRT}(0.987 \times 10^{-14})}{\gamma_{\text{NO}_3^-} \gamma_{\text{H}^+} 10^{-\text{pH}} + H_{\text{HNO}_3}^* \text{WRT}(0.987 \times 10^{-14})} \quad (\text{A2})$$

352 Where  $H_{\text{HNO}_3}^*$  is the combined molality-based equilibrium constant of HNO<sub>3</sub> dissolution and deprotonation,  $\gamma$ 's represent the  
 353 activity coefficients, W is the aerosol water, R is the gas constant, and T is the ambient temperature. Eq. A2 is equivalent  
 354 with the instantaneous calculations of ISOROPIA II within EMAC. However, the model output is produced after considering  
 355 all processes in the model and is not calculated at every timestep. Therefore, the use of Eq. 2 can provide a clearer picture of  
 356 the impact of pH on HNO<sub>3</sub> gas/particle partitioning since the model output (e.g., gas-phase HNO<sub>3</sub> and nitrate in 4 size  
 357 modes) is subject to uncertainties related to other processes (e.g., deposition, coagulation, transport, etc.).

#### 358 4.7 Sulfate formation in aqueous aerosols

359 The sulfate production rate on aqueous aerosols from the heterogeneous oxidation of S(IV) with the dissolved O<sub>3</sub> is given by

$$360 \quad R_0 = k [\text{O}_3] \quad (\text{A3})$$

361 . The first-order uptake rate,  $k$ , from monodisperse aerosols with radius  $r_a$  and total aerosol surface  $A$ , is calculated following  
 362 Jacob (Jacob, 2000):

$$363 \quad k = \left( \frac{r_a}{D_g} + \frac{4}{v\gamma} \right)^{-1} A \quad (\text{A4})$$

365 where  $v$  is the mean molecular speed of O<sub>3</sub> and  $D_g$  is its gas-phase molecular diffusion coefficient calculated as follows:

$$366 \quad D_g = \frac{9.45 \times 10^{17} \times \sqrt{T \left( 3.47 \times 10^{-2} + \frac{1}{M} \right)}}{\rho_{\text{air}}} \quad (\text{A5})$$

where  $T$  is the ambient air temperature,  $\rho_{air}$  is the air density, and  $M$  the molar mass of  $O_3$ .  $\gamma$  is the reaction probability calculated following Jacob (Jacob, 2000) and Shao et al. (Shao et al., 2019).

$$\gamma = \left( \frac{1}{\alpha} + \frac{v}{4HRT\sqrt{D_a K} f_r} \right) \quad (A6)$$

where  $\alpha$  is the mass accommodation coefficient,  $D_a$  is the aqueous-phase molecular diffusion coefficient of  $O_3$ ,  $H$  is the effective Henry's law constant of  $O_3$  (Sander, 2015),  $R$  is the ideal gas constant,  $f_r$  is the reacto-diffusive correction term (Shao et al., 2019), and  $K$  is the pseudo-first order reaction rate constant between  $S(IV)$  and  $O_3$  in the aqueous phase (Seinfeld and Pandis, 2006).

## 5. References

- Abdelkader, M., Metzger, S., Mamouri, R. E., Astitha, M., Barrie, L., Levin, Z., and Lelieveld, J.: Dust-air pollution dynamics over the eastern Mediterranean, *Atmospheric Chemistry and Physics*, 15, 9173-9189, 10.5194/acp-15-9173-2015, 2015.
- Akagi, S. K., Yokelson, R. J., Wiedinmyer, C., Alvarado, M. J., Reid, J. S., Karl, T., Crounse, J. D., and Wennberg, P. O.: Emission factors for open and domestic biomass burning for use in atmospheric models, *Atmospheric Chemistry and Physics*, 11, 4039-4072, 10.5194/acp-11-4039-2011, 2011.
- Andreae, M. O., Talbot, R. W., Andreae, T. W., and Harriss, R. C.: Formic and acetic-acid over the central Amazon region, Brazil. 1. dry season, *Journal of Geophysical Research-Atmospheres*, 93, 1616-1624, 10.1029/JD093iD02p01616, 1988.
- Ansari, A. S., and Pandis, S. N.: The effect of metastable equilibrium states on the partitioning of nitrate between the gas and aerosol phases, *Atmospheric Environment*, 34, 157-168, 10.1016/s1352-2310(99)00242-3, 2000.
- Bacer, S., Sullivan, S. C., Karydis, V. A., Barahona, D., Kramer, M., Nenes, A., Tost, H., Tsimpidi, A. P., Lelieveld, J., and Pozzer, A.: Implementation of a comprehensive ice crystal formation parameterization for cirrus and mixed-phase clouds in the EMAC model (based on MESSy 2.53), *Geoscientific Model Development*, 11, 4021-4041, 10.5194/gmd-11-4021-2018, 2018.
- Behera, S. N., Betha, R., Liu, P., and Balasubramanian, R.: A study of diurnal variations of  $PM_{2.5}$  acidity and related chemical species using a new thermodynamic equilibrium model, *Science of The Total Environment*, 452-453, 286-295, <https://doi.org/10.1016/j.scitotenv.2013.02.062>, 2013.
- Bouwman, A. F., Lee, D. S., Asman, W. A. H., Dentener, F. J., VanderHoek, K. W., and Olivier, J. G. J.: A global high-resolution emission inventory for ammonia, *Global Biogeochemical Cycles*, 11, 561-587, 10.1029/97gb02266, 1997.
- Cheng, Y. F., Zheng, G. J., Wei, C., Mu, Q., Zheng, B., Wang, Z. B., Gao, M., Zhang, Q., He, K. B., Carmichael, G., Poschl, U., and Su, H.: Reactive nitrogen chemistry in aerosol water as a source of sulfate during haze events in China, *Science Advances*, 2, 10.1126/sciadv.1601530, 2016.
- Clegg, S. L., Brimblecombe, P., and Wexler, A. S.: Thermodynamic model of the system  $H^+-NH_4^+-Na^+-SO_4^{2-}-NH_3-Cl^- - H_2O$  at 298.15 K, *J. Phys. Chem. A*, 102, 2155-2171, 10.1021/jp973043j, 1998.
- Dall'Osto, M., Ayr, R. L., Beale, R., Cree, C., Fitzsimons, M. F., Beddows, D., Harrison, R. M., Ceburnis, D., O'Dowd, C., Rinaldi, M., Paglione, M., Nenes, A., Decesari, S., and Simó, R.: Simultaneous Detection of Alkylamines in the Surface Ocean and Atmosphere of the Antarctic Sympagic Environment, *ACS Earth and Space Chemistry*, 3, 854-862, 10.1021/acsearthspacechem.9b00028, 2019.
- Dentener, F., Kinne, S., Bond, T., Boucher, O., Cofala, J., Generoso, S., Ginoux, P., Gong, S., Hoelzemann, J. J., Ito, A., Marelli, L., Penner, J. E., Putaud, J. P., Textor, C., Schulz, M., van der Werf, G. R., and Wilson, J.: Emissions of primary aerosol and precursor gases in the years 2000 and 1750 prescribed data-sets for AeroCom, *Atmos. Chem. Phys.*, 6, 4321-4344, 2006.

408 Falkovich, A. H., Graber, E. R., Schkolnik, G., Rudich, Y., Maenhaut, W., and Artaxo, P.: Low molecular weight organic  
409 acids in aerosol particles from Rondonia, Brazil, during the biomass-burning, transition and wet periods, *Atmospheric*  
410 *Chemistry and Physics*, 5, 781-797, 10.5194/acp-5-781-2005, 2005.

411 Fang, T., Guo, H. Y., Zeng, L. H., Verma, V., Nenes, A., and Weber, R. J.: Highly Acidic Ambient Particles, Soluble  
412 Metals, and Oxidative Potential: A Link between Sulfate and Aerosol Toxicity, *Environmental Science & Technology*,  
413 51, 2611-2620, 10.1021/acs.est.6b06151, 2017.

414 Fountoukis, C., and Nenes, A.: ISORROPIA II: a computationally efficient thermodynamic equilibrium model for  $K^+$ - $Ca^{2+}$ -  
415  $Mg^{2+}$ - $NH_4^+$ - $Na^+$ - $SO_4^{2-}$ - $NO_3^-$ - $Cl^-$ - $H_2O$  aerosols, *Atmospheric Chemistry and Physics*, 7, 4639-4659, 2007.

416 Friese, E., and Ebel, A.: Temperature Dependent Thermodynamic Model of the System  
417  $H^+$ - $NH_4^+$ - $Na^+$ - $SO_4^{2-}$ - $NO_3^-$ - $Cl^-$ - $H_2O$ , *The Journal of Physical Chemistry A*, 114, 11595-11631,  
418 10.1021/jp101041j, 2010.

419 Grewe, V., Brunner, D., Dameris, M., Grenfell, J. L., Hein, R., Shindell, D., and Staehelin, J.: Origin and variability of upper  
420 tropospheric nitrogen oxides and ozone at northern mid-latitudes, *Atmospheric Environment*, 35, 3421-3433,  
421 10.1016/s1352-2310(01)00134-0, 2001.

422 Guo, H., Xu, L., Bougiatioti, A., Cerully, K. M., Capps, S. L., Hite, J. R., Carlton, A. G., Lee, S. H., Bergin, M. H., Ng, N.  
423 L., Nenes, A., and Weber, R. J.: Fine-particle water and pH in the southeastern United States, *Atmospheric Chemistry*  
424 *and Physics*, 15, 5211-5228, 10.5194/acp-15-5211-2015, 2015.

425 Guo, H., Sullivan, A. P., Campuzano-Jost, P., Schroder, J. C., Lopez-Hilfiker, F. D., Dibb, J. E., Jimenez, J. L., Thornton, J.  
426 A., Brown, S. S., Nenes, A., and Weber, R. J.: Fine particle pH and the partitioning of nitric acid during winter in the  
427 northeastern United States, *Journal of Geophysical Research-Atmospheres*, 121, 10355-10376, 10.1002/2016jd025311,  
428 2016.

429 Guo, H., Otjes, R., Schlag, P., Kiendler-Scharr, A., Nenes, A., and Weber, R. J.: Effectiveness of ammonia reduction on  
430 control of fine particle nitrate, *Atmospheric Chemistry and Physics*, 18, 12241-12256, 10.5194/acp-18-12241-2018,  
431 2018.

432 Guo, H. Y., Liu, J. M., Froyd, K. D., Roberts, J. M., Veres, P. R., Hayes, P. L., Jimenez, J. L., Nenes, A., and Weber, R. J.:  
433 Fine particle pH and gas-particle phase partitioning of inorganic species in Pasadena, California, during the 2010 CalNex  
434 campaign, *Atmospheric Chemistry and Physics*, 17, 5703-5719, 10.5194/acp-17-5703-2017, 2017.

435 Hennigan, C. J., Izumi, J., Sullivan, A. P., Weber, R. J., and Nenes, A.: A critical evaluation of proxy methods used to  
436 estimate the acidity of atmospheric particles, *Atmospheric Chemistry and Physics*, 15, 2775-2790, 10.5194/acp-15-2775-  
437 2015, 2015.

438 Jacob, D. J.: Heterogeneous chemistry and tropospheric ozone, *Atmospheric Environment*, 34, 2131-2159, 10.1016/s1352-  
439 2310(99)00462-8, 2000.

440 Jensen, J.: On the convex functions and inequalities between mean values, *Acta Mathematica*, 30, 175-193,  
441 10.1007/bf02418571, 1906.

442 Jia, S., Wang, X., Zhang, Q., Sarkar, S., Wu, L., Huang, M., Zhang, J., and Yang, L.: Technical note: Comparison and  
443 interconversion of pH based on different standard states for aerosol acidity characterization, *Atmos. Chem. Phys.*, 18,  
444 11125-11133, 10.5194/acp-18-11125-2018, 2018.

445 Jickells, T. D., An, Z. S., Andersen, K. K., Baker, A. R., Bergametti, G., Brooks, N., Cao, J. J., Boyd, P. W., Duce, R. A.,  
446 Hunter, K. A., Kawahata, H., Kubilay, N., laRoche, J., Liss, P. S., Mahowald, N., Prospero, J. M., Ridgwell, A. J., Tegen,  
447 I., and Torres, R.: Global iron connections between desert dust, ocean biogeochemistry, and climate, *Science*, 308, 67-71,  
448 10.1126/science.1105959, 2005.

449 Jöckel, P., Tost, H., Pozzer, A., Bruehl, C., Buchholz, J., Ganzeveld, L., Hoor, P., Kerkweg, A., Lawrence, M. G., Sander,  
450 R., Steil, B., Stiller, G., Tanarhte, M., Taraborrelli, D., Van Aardenne, J., and Lelieveld, J.: The atmospheric chemistry  
451 general circulation model ECHAM5/MESSy1: consistent simulation of ozone from the surface to the mesosphere,  
452 *Atmos. Chem. Phys.*, 6, 5067-5104, 2006.

453 Jöckel, P., Kerkweg, A., Pozzer, A., Sander, R., Tost, H., Riede, H., Baumgaertner, A., Gromov, S., and Kern, B.:  
454 Development cycle 2 of the Modular Earth Submodel System (MESSy2), *Geoscientific Model Development*, 3, 717-752,  
455 2010.

456 Karydis, V. A., Tsimpidi, A. P., Pozzer, A., Astitha, M., and Lelieveld, J.: Effects of mineral dust on global atmospheric  
457 nitrate concentrations, *Atmos. Chem. Phys.*, 16, 1491-1509, 10.5194/acp-16-1491-2016, 2016.

458 Karydis, V. A., Tsimpidi, A. P., Bacer, S., Pozzer, A., Nenes, A., and Lelieveld, J.: Global impact of mineral dust on cloud  
459 droplet number concentration, *Atmospheric Chemistry and Physics*, 17, 5601-5621, 10.5194/acp-17-5601-2017, 2017.

460 Kerkweg, A., Buchholz, J., Ganzeveld, L., Pozzer, A., Tost, H., and Jöckel, P.: Technical Note: An implementation of the  
461 dry removal processes DRY DEPosition and SEDimentation in the Modular Earth Submodel System (MESSy), *Atmos.*  
462 *Chem. Phys.*, 6, 4617-4632, 2006.

463 Klingmüller, K., Metzger, S., Abdelkader, M., Karydis, V. A., Stenchikov, G. L., Pozzer, A., and Lelieveld, J.: Revised  
464 mineral dust emissions in the atmospheric chemistry-climate model EMAC (MESSy 2.52 DU\_Astithal KKDU2017  
465 patch), *Geoscientific Model Development*, 11, 989-1008, 10.5194/gmd-11-989-2018, 2018.

466 Klingmüller, K., Lelieveld, J., Karydis, V. A., and Stenchikov, G. L.: Direct radiative effect of dust-pollution interactions,  
467 *Atmospheric Chemistry and Physics*, 19, 7397-7408, 10.5194/acp-19-7397-2019, 2019.

468 Klingmüller, K., Karydis, V. A., Bacer, S., Stenchikov, G. L., and Lelieveld, J.: Weaker cooling by aerosols due to dust-  
469 pollution interactions, *Atmos. Chem. Phys. Discuss.*, 2020, 1-19, 10.5194/acp-2020-531, 2020.

470 Lawal, A. S., Guan, X. B., Liu, C., Henneman, L. R. F., Vasilakos, P., Bhogineni, V., Weber, R. J., Nenes, A., and Russell,  
471 A. G.: Linked Response of Aerosol Acidity and Ammonia to SO<sub>2</sub> and NO<sub>x</sub> Emissions Reductions in the United States,  
472 *Environmental Science & Technology*, 52, 9861-9873, 10.1021/acs.est.8b00711, 2018.

473 Lelieveld, J., Evans, J. S., Fnais, M., Giannadaki, D., and Pozzer, A.: The contribution of outdoor air pollution sources to  
474 premature mortality on a global scale, *Nature*, 525, 367-371, 10.1038/nature15371, 2015.

475 Leygraf, C., Wallinder, I. O., Tidblad, J., and Graedel, T.: *Atmospheric Corrosion*, John Wiley & Sons, 2016.

476 Li, C., McLinden, C., Fioletov, V., Krotkov, N., Carn, S., Joiner, J., Streets, D., He, H., Ren, X., Li, Z., and Dickerson, R. R.:  
477 India Is Overtaking China as the World's Largest Emitter of Anthropogenic Sulfur Dioxide, *Scientific Reports*, 7, 14304,  
478 10.1038/s41598-017-14639-8, 2017.

479 Lohmann, U., and Ferrachat, S.: Impact of parametric uncertainties on the present-day climate and on the anthropogenic  
480 aerosol effect, *Atmos. Chem. Phys.*, 10, 11373-11383, 10.5194/acp-10-11373-2010, 2010.

481 Marais, E. A., Jacob, D. J., Jimenez, J. L., Campuzano-Jost, P., Day, D. A., Hu, W., Krechmer, J., Zhu, L., Kim, P. S.,  
482 Miller, C. C., Fisher, J. A., Travis, K., Yu, K., Hanisco, T. F., Wolfe, G. M., Arkinson, H. L., Pye, H. O. T., Froyd, K. D.,  
483 Liao, J., and McNeill, V. F.: Aqueous-phase mechanism for secondary organic aerosol formation from isoprene:  
484 application to the southeast United States and co-benefit of SO<sub>2</sub> emission controls, *Atmospheric Chemistry and Physics*,  
485 16, 1603-1618, 10.5194/acp-16-1603-2016, 2016.

486 Masiol, M., Squizzato, S., Formenton, G., Khan, M. B., Hopke, P. K., Nenes, A., Pandis, S. N., Tositti, L., Benetello, F.,  
487 Visin, F., and Pavoni, B.: Hybrid multiple-site mass closure and source apportionment of PM<sub>2.5</sub> and aerosol acidity at  
488 major cities in the Po Valley, *Science of The Total Environment*, 704, 135287,  
489 <https://doi.org/10.1016/j.scitotenv.2019.135287>, 2020.

490 McCormick, M. P., Thomason, L. W., and Trepte, C. R.: ATMOSPHERIC EFFECTS OF THE MT-PINATUBO  
491 ERUPTION, *Nature*, 373, 399-404, 10.1038/373399a0, 1995.

492 Meng, Z. Y., Seinfeld, J. H., Saxena, P., and Kim, Y. P.: Atmospheric gas-aerosol equilibrium .4. Thermodynamics of  
493 carbonates, *Aerosol Science and Technology*, 23, 131-154, 1995.

494 Meng, Z. Y., and Seinfeld, J. H.: Time scales to achieve atmospheric gas-aerosol equilibrium for volatile species,  
495 *Atmospheric Environment*, 30, 2889-2900, 10.1016/1352-2310(95)00493-9, 1996.

496 Metzger, S., Mihalopoulos, N., and Lelieveld, J.: Importance of mineral cations and organics in gas-aerosol partitioning of  
497 reactive nitrogen compounds: case study based on MINOS results, *Atmospheric Chemistry and Physics*, 6, 2549-2567,  
498 10.5194/acp-6-2549-2006, 2006.

499 Nah, T., Guo, H., Sullivan, A. P., Chen, Y., Tanner, D. J., Nenes, A., Russell, A., Ng, N. L., Huey, L. G., and Weber, R. J.:  
500 Characterization of aerosol composition, aerosol acidity, and organic acid partitioning at an agriculturally intensive rural  
501 southeastern US site, *Atmos. Chem. Phys.*, 18, 11471-11491, 10.5194/acp-18-11471-2018, 2018.

502 Nenes, A., Pandis, S. N., Weber, R. J., and Russell, A.: Aerosol pH and liquid water content determine when particulate  
503 matter is sensitive to ammonia and nitrate availability, *Atmospheric Chemistry and Physics*, 20, 3249-3258, 10.5194/acp-  
504 20-3249-2020, 2020.

505 Oakes, M., Ingall, E. D., Lai, B., Shafer, M. M., Hays, M. D., Liu, Z. G., Russell, A. G., and Weber, R. J.: Iron Solubility  
506 Related to Particle Sulfur Content in Source Emission and Ambient Fine Particles, *Environmental Science &*  
507 *Technology*, 46, 6637-6644, 10.1021/es300701c, 2012.

508 Park, M., Joo, H. S., Lee, K., Jang, M., Kim, S. D., Kim, I., Borlaza, L. J. S., Lim, H., Shin, H., Chung, K. H., Choi, Y.-H.,  
 509 Park, S. G., Bae, M.-S., Lee, J., Song, H., and Park, K.: Differential toxicities of fine particulate matters from various  
 510 sources, *Scientific Reports*, 8, 17007, 10.1038/s41598-018-35398-0, 2018.  
 511 Pathak, R. K., Yao, X. H., and Chan, C. K.: Sampling artifacts of acidity and ionic species in PM<sub>2.5</sub>, *Environmental Science*  
 512 & *Technology*, 38, 254-259, 10.1021/es0342244, 2004.  
 513 Pathak, R. K., Wu, W. S., and Wang, T.: Summertime PM<sub>2.5</sub> ionic species in four major cities of China: nitrate  
 514 formation in an ammonia-deficient atmosphere, *Atmos. Chem. Phys.*, 9, 1711-1722, 10.5194/acp-9-1711-2009, 2009.  
 515 Petters, M. D., and Kreidenweis, S. M.: A single parameter representation of hygroscopic growth and cloud condensation  
 516 nucleus activity, *Atmospheric Chemistry and Physics*, 7, 1961-1971, 2007.  
 517 Pozzer, A., Joeckel, P. J., Sander, R., Williams, J., Ganzeveld, L., and Lelieveld, J.: Technical note: the MESSy-submodel  
 518 AIRSEA calculating the air-sea exchange of chemical species, *Atmos. Chem. Phys.*, 6, 5435-5444, 2006.  
 519 Pozzer, A., Jockel, P., and Van Aardenne, J.: The influence of the vertical distribution of emissions on tropospheric  
 520 chemistry, *Atmospheric Chemistry and Physics*, 9, 9417-9432, 2009.  
 521 Pozzer, A., de Meij, A., Pringle, K. J., Tost, H., Doering, U. M., van Aardenne, J., and Lelieveld, J.: Distributions and  
 522 regional budgets of aerosols and their precursors simulated with the EMAC chemistry-climate model, *Atmos. Chem.*  
 523 *Phys.*, 12, 961-987, 2012.  
 524 Pozzer, A., Tsimpidi, A. P., Karydis, V. A., de Meij, A., and Lelieveld, J.: Impact of agricultural emission reductions on  
 525 fine-particulate matter and public health, *Atmospheric Chemistry and Physics*, 17, 12813-12826, 10.5194/acp-17-12813-  
 526 2017, 2017.  
 527 Pringle, K. J., Tost, H., Message, S., Steil, B., Giannadaki, D., Nenes, A., Fountoukis, C., Stier, P., Vignati, E., and Lelieveld, J.:  
 528 Description and evaluation of GMX: a new aerosol submodel for global simulations (v1), *Geoscientific Model*  
 529 *Development*, 3, 391-412, 2010.  
 530 Pye, H. O. T., Nenes, A., Alexander, B., Ault, A. P., Barth, M. C., Clegg, S. L., Collett, J. L., Fahey, K. M., Hennigan, C. J.,  
 531 Herrmann, H., Kanakidou, M., Kelly, J. T., Ku, I. T., McNeill, V. F., Riemer, N., Schaefer, T., Shi, G. L., Tilgner, A.,  
 532 Walker, J. T., Wang, T., Weber, R., Xing, J., Zaveri, R. A., and Zuend, A.: The acidity of atmospheric particles and  
 533 clouds, *Atmospheric Chemistry and Physics*, 20, 4809-4888, 10.5194/acp-20-4809-2020, 2020.  
 534 Raizenne, M., Neas, L. M., Damokosh, A. I., Dockery, D. W., Spengler, J. D., Koutrakis, P., Ware, J. H., and Speizer, F. E.:  
 535 Health effects of acid aerosols on North American children: Pulmonary function, *Environmental Health Perspectives*,  
 536 104, 506-514, 10.2307/3432991, 1996.  
 537 Roeckner, E., Brokopf, R., Esch, M., Giorgetta, M., Hagemann, S., Kornbluh, L., Manzini, E., Schlese, U., and  
 538 Schulzweida, U.: Sensitivity of simulated climate to horizontal and vertical resolution in the ECHAM5 atmosphere  
 539 model, *Journal of Climate*, 19, 3771-3791, 10.1175/jcli3824.1, 2006.  
 540 Saiz-Lopez, A., and von Glasow, R.: Reactive halogen chemistry in the troposphere, *Chemical Society Reviews*, 41, 6448-  
 541 6472, 10.1039/c2cs35208g, 2012.  
 542 Sander, R.: Compilation of Henry's law constants (version 4.0) for water as solvent, *Atmos. Chem. Phys.*, 15, 4399-4981,  
 543 10.5194/acp-15-4399-2015, 2015.  
 544 Sander, R., Baumgaertner, A., Cabrera-Perez, D., Frank, F., Gromov, S., Grooss, J. U., Harder, H., Huijnen, V., Jockel, P.,  
 545 Karydis, V. A., Niemeyer, K. E., Pozzer, A., Hella, R. B., Schultz, M. G., Taraborrelli, D., and Tauer, S.: The community  
 546 atmospheric chemistry box model CAABA/MECCA-4.0, *Geoscientific Model Development*, 12, 1365-1385,  
 547 10.5194/gmd-12-1365-2019, 2019.  
 548 Schaap, M., van Loon, M., ten Brink, H. M., Dentener, F. J., and Builtjes, P. J. H.: Secondary inorganic aerosol simulations  
 549 for Europe with special attention to nitrate, *Atmos. Chem. Phys.*, 4, 857-874, 10.5194/acp-4-857-2004, 2004.  
 550 Seinfeld, J. H., and Pandis, S. N.: *Atmospheric Chemistry and Physics: From Air Pollution to Climate Change*, Second ed.,  
 551 John Wiley & Sons, Inc., Hoboken, New Jersey, 2006.  
 552 Shao, J., Chen, Q., Wang, Y., Lu, X., He, P., Sun, Y., Shah, V., Martin, R. V., Philip, S., Song, S., Zhao, Y., Xie, Z., Zhang,  
 553 L., and Alexander, B.: Heterogeneous sulfate aerosol formation mechanisms during wintertime Chinese haze events: air  
 554 quality model assessment using observations of sulfate oxygen isotopes in Beijing, *Atmos. Chem. Phys.*, 19, 6107-6123,  
 555 10.5194/acp-19-6107-2019, 2019.



Shi, G., Xu, J., Peng, X., Xiao, Z., Chen, K., Tian, Y., Guan, X., Feng, Y., Yu, H., Nenes, A., and Russell, A. G.: pH of Aerosols in a Polluted Atmosphere: Source Contributions to Highly Acidic Aerosol, *Environmental Science & Technology*, 51, 4289-4296, 10.1021/acs.est.6b05736, 2017.

Song, S., Gao, M., Xu, W., Shao, J., Shi, G., Wang, S., Wang, Y., Sun, Y., and McElroy, M. B.: Fine-particle pH for Beijing winter haze as inferred from different thermodynamic equilibrium models, *Atmos. Chem. Phys.*, 18, 7423-7438, 10.5194/acp-18-7423-2018, 2018.

Squizzato, S., Masiol, M., Brunelli, A., Pistollato, S., Tarabotti, E., Rampazzo, G., and Pavoni, B.: Factors determining the formation of secondary inorganic aerosol: a case study in the Po Valley (Italy), *Atmos. Chem. Phys.*, 13, 1927-1939, 10.5194/acp-13-1927-2013, 2013.

Sullivan, R. C., Moore, M. J. K., Petters, M. D., Kreidenweis, S. M., Roberts, G. C., and Prather, K. A.: Effect of chemical mixing state on the hygroscopicity and cloud nucleation properties of calcium mineral dust particles, *Atmospheric Chemistry and Physics*, 9, 3303-3316, 2009.

Surratt, J. D., Chan, A. W. H., Eddingsaas, N. C., Chan, M. N., Loza, C. L., Kwan, A. J., Hersey, S. P., Flagan, R. C., Wennberg, P. O., and Seinfeld, J. H.: Reactive intermediates revealed in secondary organic aerosol formation from isoprene, *Proceedings of the National Academy of Sciences of the United States of America*, 107, 6640-6645, 10.1073/pnas.0911114107, 2010.

Tan, T., Hu, M., Li, M., Guo, Q., Wu, Y., Fang, X., Gu, F., Wang, Y., and Wu, Z.: New insight into PM<sub>2.5</sub> pollution patterns in Beijing based on one-year measurement of chemical compositions, *Science of The Total Environment*, 621, 734-743, <https://doi.org/10.1016/j.scitotenv.2017.11.208>, 2018.

Tost, H., Jockel, P. J., Kerkweg, A., Sander, R., and Lelieveld, J.: Technical note: A new comprehensive SCAVenging submodel for global atmospheric chemistry modelling, *Atmos. Chem. Phys.*, 6, 565-574, 2006.

Tsimpidi, A. P., Karydis, V. A., Pozzer, A., Pandis, S. N., and Lelieveld, J.: ORACLE (v1.0): module to simulate the organic aerosol composition and evolution in the atmosphere, *Geoscientific Model Development*, 7, 3153-3172, 10.5194/gmd-7-3153-2014, 2014.

Tsimpidi, A. P., Karydis, V. A., Pandis, S. N., and Lelieveld, J.: Global combustion sources of organic aerosols: model comparison with 84 AMS factor-analysis data sets, *Atmos. Chem. Phys.*, 16, 8939-8962, 10.5194/acp-16-8939-2016, 2016.

Tsimpidi, A. P., Karydis, V. A., Pozzer, A., Pandis, S. N., and Lelieveld, J.: ORACLE 2-D (v2.0): an efficient module to compute the volatility and oxygen content of organic aerosol with a global chemistry-climate model, *Geoscientific Model Development*, 11, 3369-3389, 10.5194/gmd-11-3369-2018, 2018.

van Vuuren, D. P., Edmonds, J., Kainuma, M., Riahi, K., Thomson, A., Hibbard, K., Hurtt, G. C., Kram, T., Krey, V., Lamarque, J. F., Masui, T., Meinshausen, M., Nakicenovic, N., Smith, S. J., and Rose, S. K.: The representative concentration pathways: an overview, *Climatic Change*, 109, 5-31, 10.1007/s10584-011-0148-z, 2011.

Vieira-Filho, M., Pedrotti, J. J., and Fornaro, A.: Water-soluble ions species of size-resolved aerosols: Implications for the atmospheric acidity in São Paulo megacity, Brazil, *Atmospheric Research*, 181, 281-287, <https://doi.org/10.1016/j.atmosres.2016.07.006>, 2016.

Vignati, E., Wilson, J., and Stier, P.: M7: An efficient size-resolved aerosol microphysics module for large-scale aerosol transport models, *J. Geophys. Res.-Atmos.*, 109, doi: 10.1029/2003jd004485, 2004.

Wang, H., Ding, J., Xu, J., Wen, J., Han, J., Wang, K., Shi, G., Feng, Y., Ivey, C. E., Wang, Y., Nenes, A., Zhao, Q., and Russell, A. G.: Aerosols in an arid environment: The role of aerosol water content, particulate acidity, precursors, and relative humidity on secondary inorganic aerosols, *Science of The Total Environment*, 646, 564-572, <https://doi.org/10.1016/j.scitotenv.2018.07.321>, 2019a.

Wang, Y., Li, W., Gao, W., Liu, Z., Tian, S., Shen, R., Ji, D., Wang, S., Wang, L., Tang, G., Song, T., Cheng, M., Wang, G., Gong, Z., Hao, J., and Zhang, Y.: Trends in particulate matter and its chemical compositions in China from 2013–2017, *Science China Earth Sciences*, 62, 1857-1871, 10.1007/s11430-018-9373-1, 2019b.

Weber, R. J., Guo, H. Y., Russell, A. G., and Nenes, A.: High aerosol acidity despite declining atmospheric sulfate concentrations over the past 15 years, *Nature Geoscience*, 9, 282-285, 10.1038/ngeo2665, 2016.

Xu, L., Guo, H. Y., Boyd, C. M., Klein, M., Bougiatioti, A., Cerully, K. M., Hite, J. R., Isaacman-VanWertz, G., Kreisberg, N. M., Knote, C., Olson, K., Koss, A., Goldstein, A. H., Hering, S. V., de Gouw, J., Baumann, K., Lee, S. H., Nenes, A., Weber, R. J., and Ng, N. L.: Effects of anthropogenic emissions on aerosol formation from isoprene and monoterpenes in

606 the southeastern United States, *Proceedings of the National Academy of Sciences of the United States of America*, 112,  
607 37-42, 10.1073/pnas.1417609112, 2015.

608 Xue, J., Lau, A. K. H., and Yu, J. Z.: A study of acidity on PM<sub>2.5</sub> in Hong Kong using online ionic chemical composition  
609 measurements, *Atmospheric Environment*, 45, 7081-7088, <https://doi.org/10.1016/j.atmosenv.2011.09.040>, 2011.

610 Yao, X., Ling, T. Y., Fang, M., and Chan, C. K.: Size dependence of in situ pH in submicron atmospheric particles in Hong  
611 Kong, *Atmospheric Environment*, 41, 382-393, <https://doi.org/10.1016/j.atmosenv.2006.07.037>, 2007.

612 Yienger, J. J., and Levy, H.: Empirical-model of global soil-biogenic NO<sub>x</sub> emissions, *Journal of Geophysical Research-*  
613 *Atmospheres*, 100, 11447-11464, 10.1029/95jd00370, 1995.

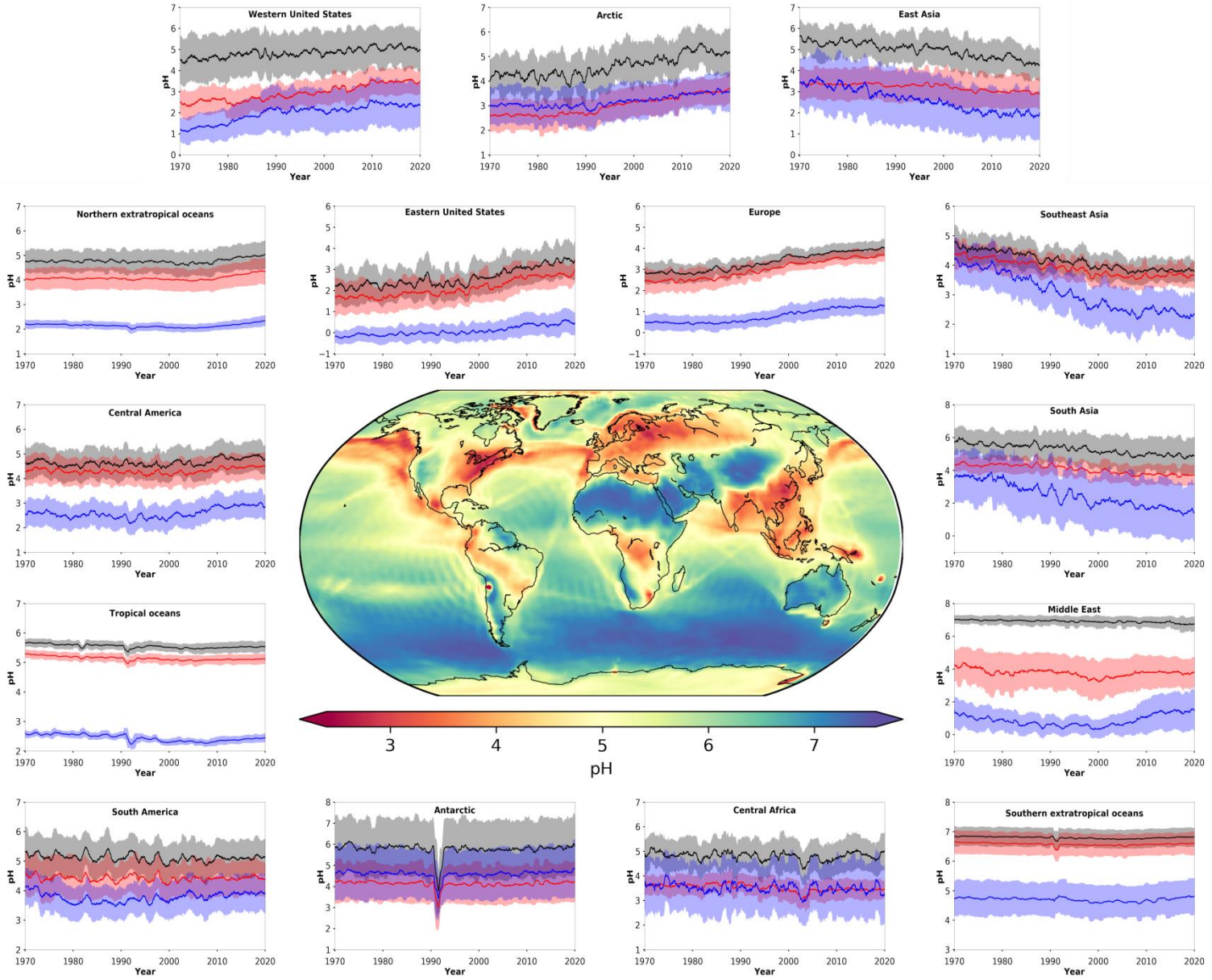
614 Zakoura, M., Kakavas, S., Nenes, A., and Pandis, S. N.: Size-resolved aerosol pH over Europe during summer, *Atmos.*  
615 *Chem. Phys. Discuss.*, 2020, 1-24, 10.5194/acp-2019-1146, 2020.

616 Zheng, G., Su, H., Wang, S., Andreae, M. O., Pöschl, U., and Cheng, Y.: Multiphase buffer theory explains contrasts in  
617 atmospheric aerosol acidity, *Science*, 369, 1374-1377, 10.1126/science.aba3719, 2020.

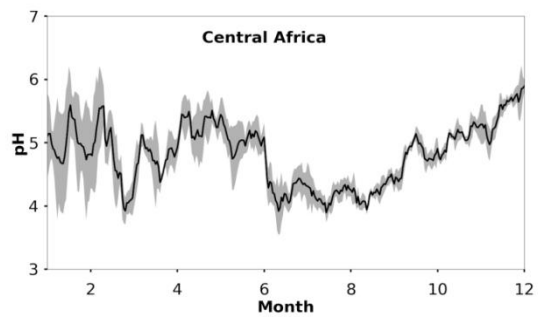
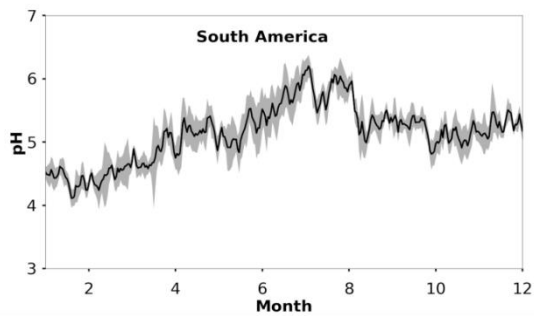
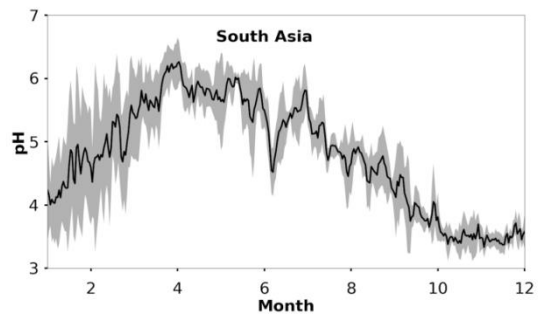
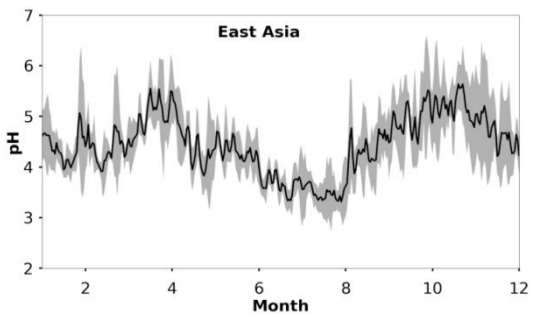
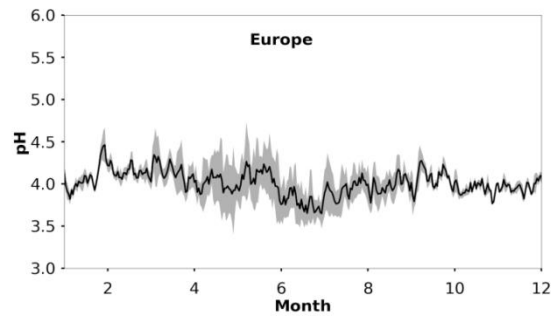
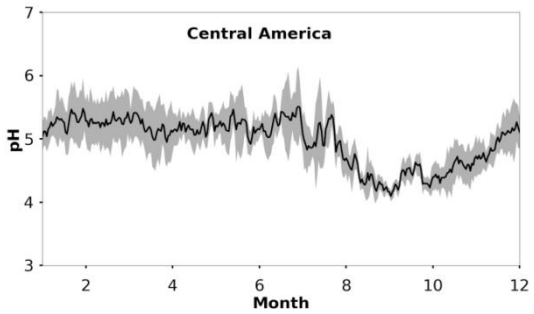
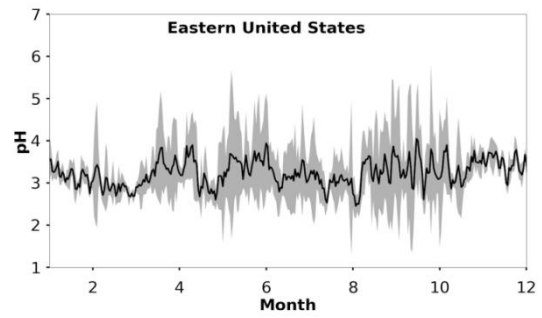
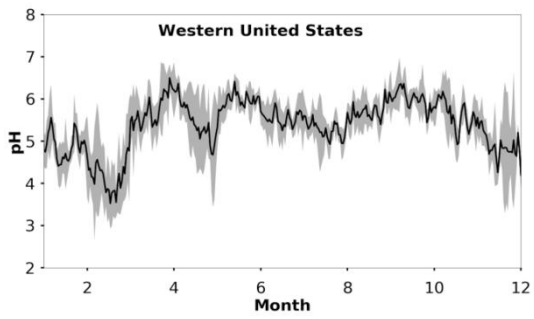
619

620 **Author contributions:** V.A.K. and J.L. planned the research, V.A.K., A.P.T. and A.P. performed the model calculations,  
621 V.A.K., A.P., and J.L. analyzed the results, V.A.K. and J.L. wrote the paper. All authors contributed to the manuscript.;

622 **Competing interests:** Authors declare no competing interests. **Code/Data availability:** Data and related material can be  
623 obtained from V.A.K. ([v.karydis@fz-juelich.de](mailto:v.karydis@fz-juelich.de)) upon request.



**Figure 1: Mean, near-surface fine aerosol pH during the period 2010-2015 (central panel). Surrounding panels show the temporal pH evolution during the period 1970-2020 at locations defined in Table 1. Black lines represent the reference simulation. Red and blue lines show the sensitivity simulations in which crustal particle and  $\text{NH}_3$  emissions are removed, respectively. Ranges represent the  $1\sigma$  standard deviation. The anomaly in 1991/2 is related to the Mt Pinatubo eruption.**



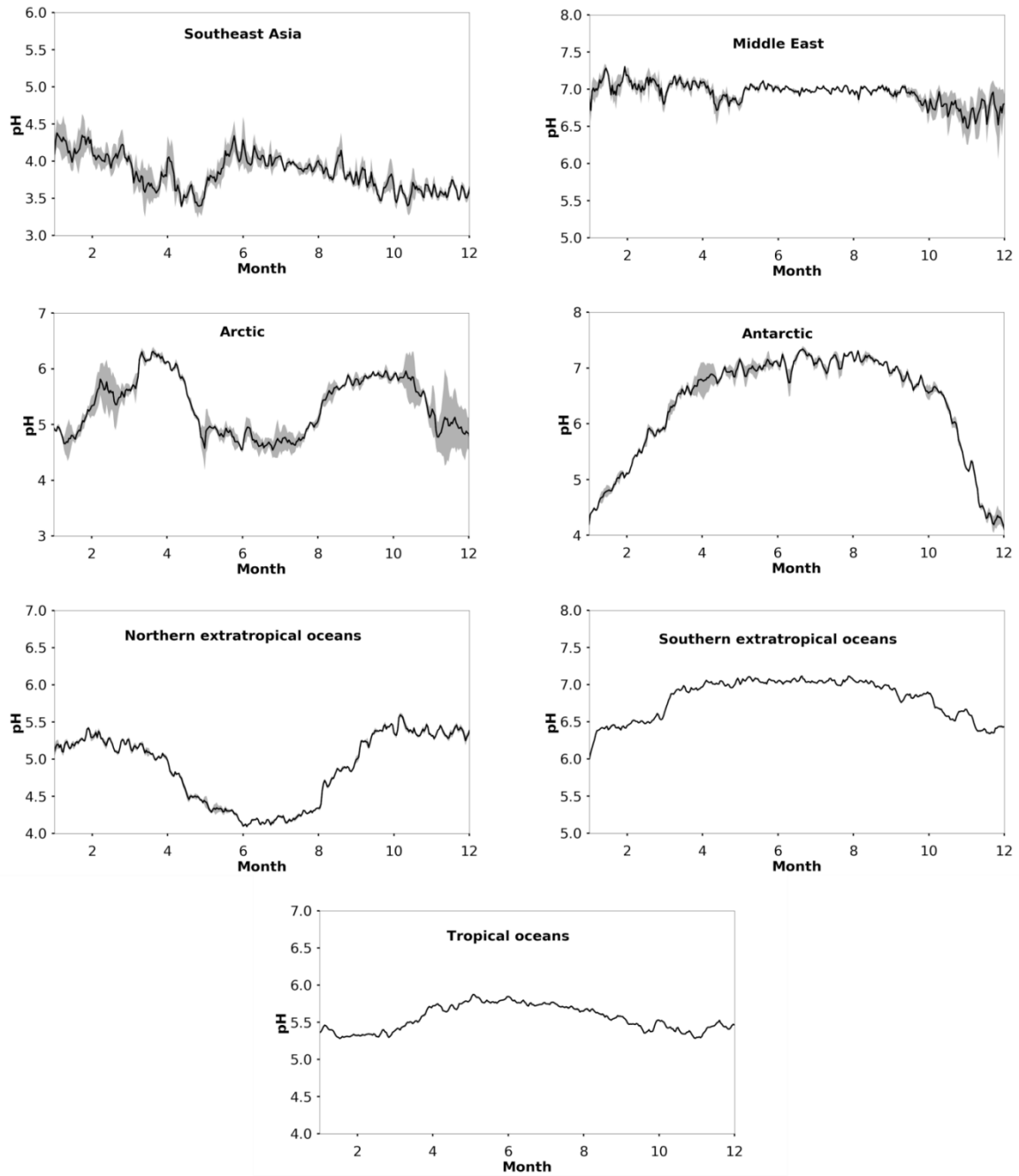


**Figure 2: Average seasonal cycle of modelled pH during the period 2010-2015 at locations defined in Table 1. Ranges represent the  $1\sigma$  standard deviation.**

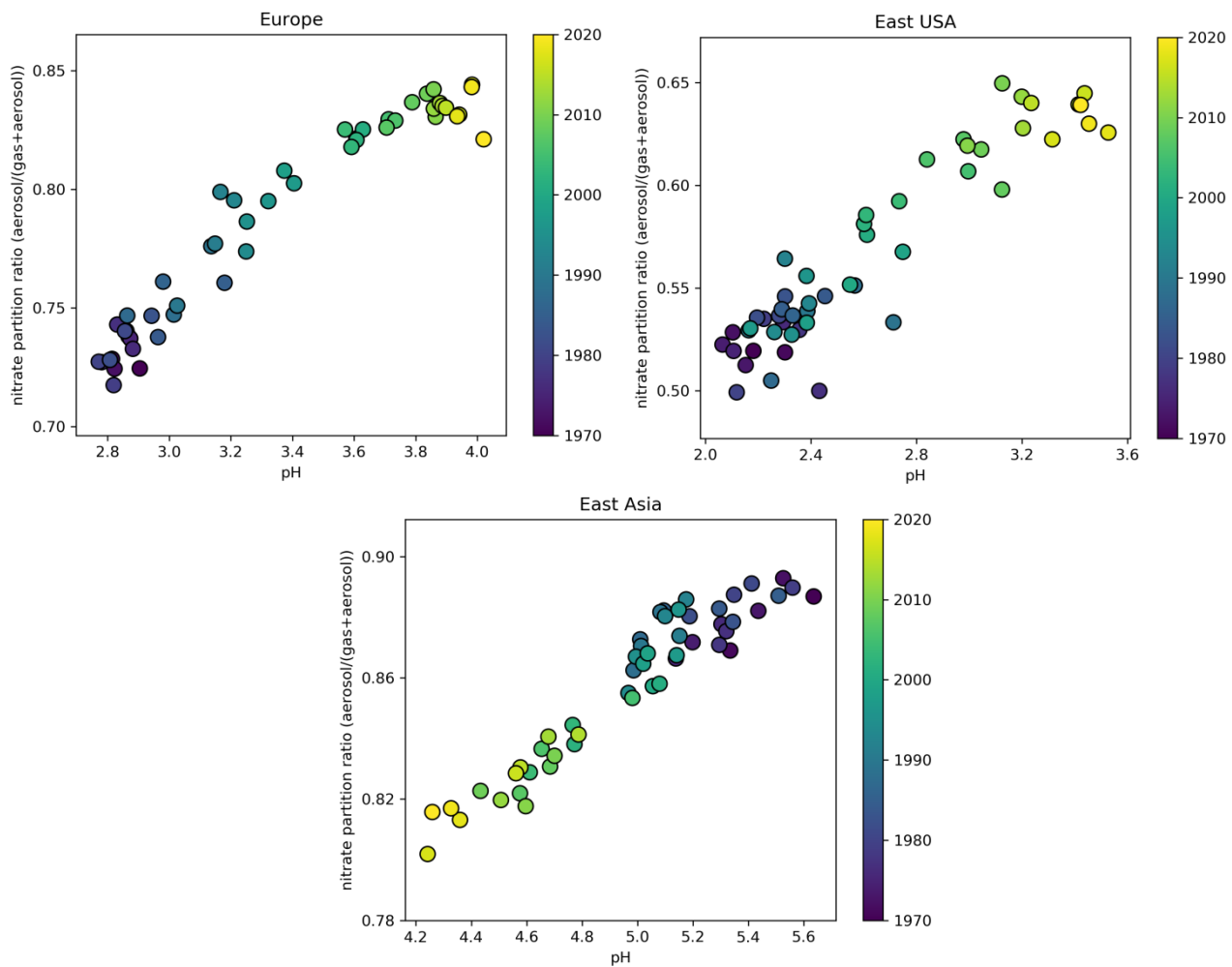


**Figure 3: Time evolution of particle phase fraction of total nitrate as a function of pH over Europe (left), the Eastern USA (right) and East Asia (bottom) during the period 1970-2020.**

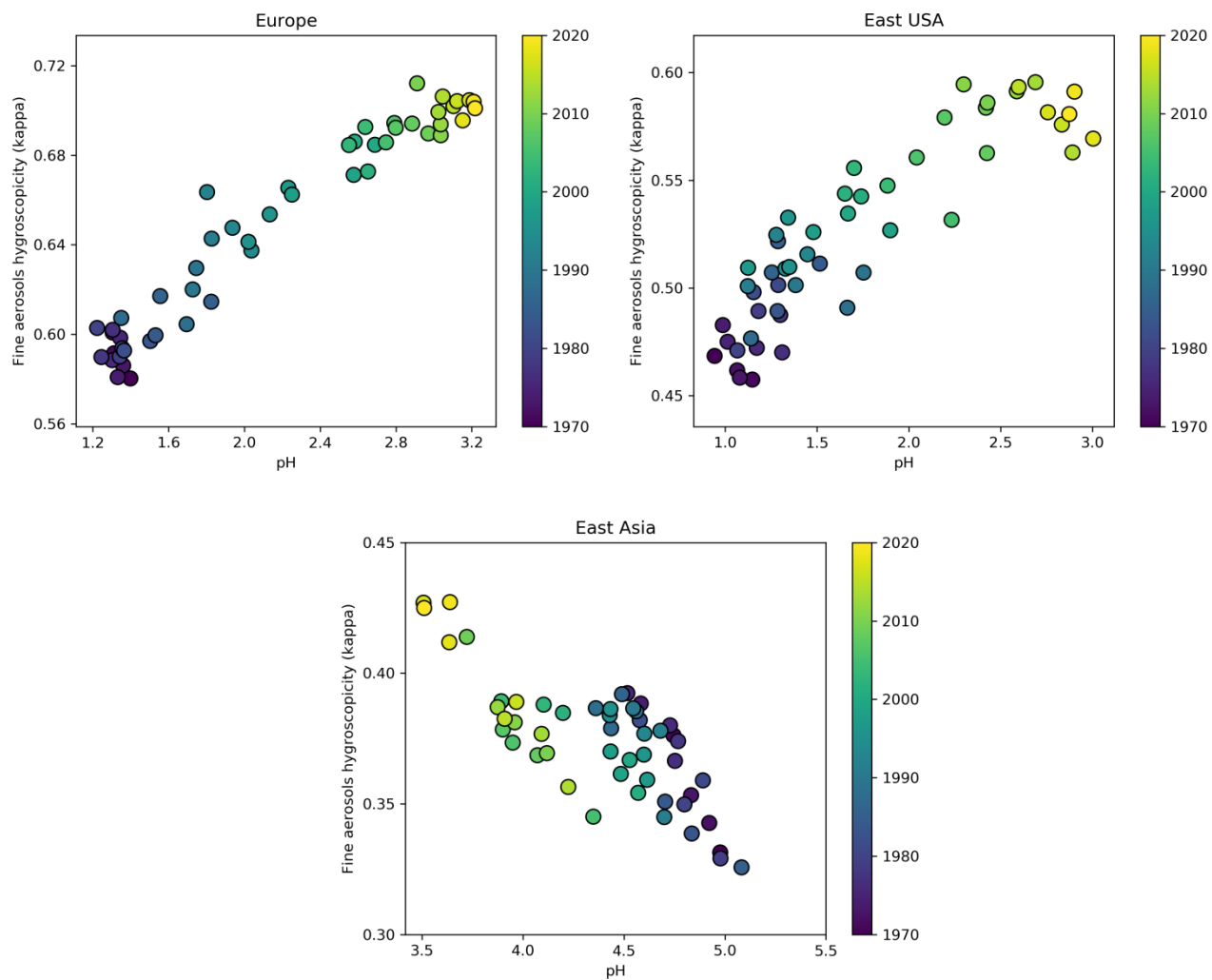


**Figure 4: Time evolution of annual average aerosol hygroscopicity ( $\kappa$ ) as a function of pH over Europe (left), the Eastern USA (right) and East Asia (bottom) during the period 1970-2020 at the lowest cloud-forming level (940 hPa).**

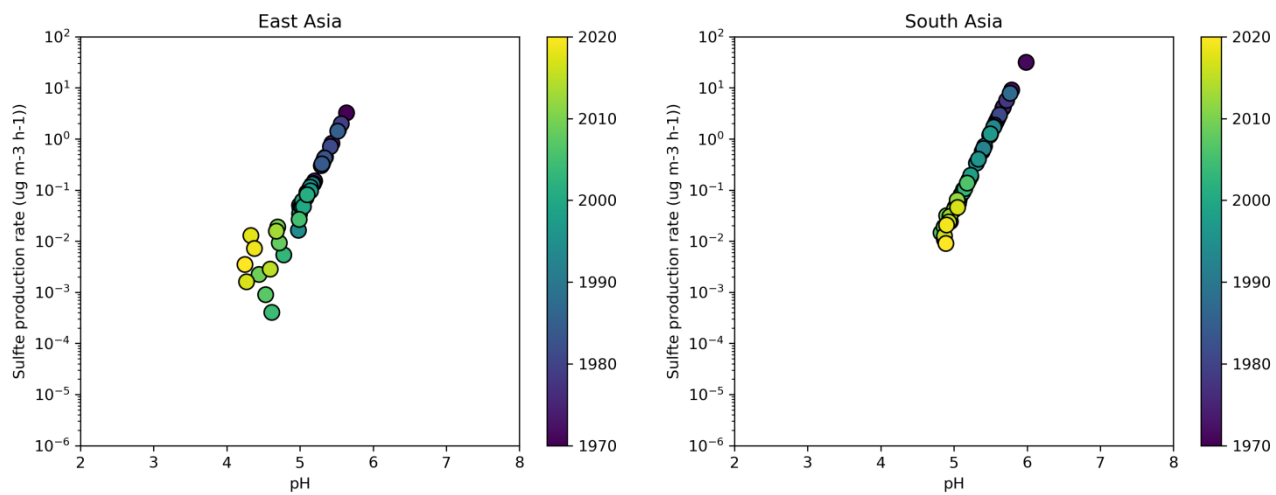


**Figure 5: Time evolution of the sulfate production rate on aqueous aerosols from the  $\text{SO}_2+\text{O}_3$  multiphase chemistry reaction as a function of aerosol pH over East Asia (left) and South Asia (right) during the period 1970-2020.**



**Table 1: Decadal averages of aerosol pH.**

Region	Longitude	Latitude	1971-1980	1981-1990	1991-2000	2001-2010	2011-2020
Western USA <sup>1</sup>	90°-70°W	30°-46°N	4.6	4.8	4.8	5.0	5.1
Eastern USA <sup>1</sup>	124°-114°W	30°-52°N	2.2	2.4	2.4	2.9	3.3
Central America <sup>1</sup>	106°-52°W	4°-28°N	4.6	4.6	4.6	4.7	4.9
Europe <sup>1</sup>	12°W-36°E	34°-62°N	2.8	3.0	3.3	3.7	3.9
East Asia <sup>1</sup>	100°-114°E	20°-44°N	5.3	5.2	5.1	4.7	4.5
South Asia <sup>1</sup>	68°-94°E	8°-32°N	5.6	5.5	5.3	5.0	4.9
South America <sup>1</sup>	75°-35°W	30°-0°S	5.2	5.1	5.1	5.1	5.1
Central Africa <sup>1</sup>	10°-40°E	10°S-10°N	4.9	4.8	4.8	4.7	4.9
Southeast Asia <sup>1</sup>	94°-130°E	12°S-20°N	4.5	4.3	4.1	3.9	3.8
Middle East <sup>1</sup>	36°-60°E	12°-34°N	7.0	7.0	6.9	6.9	6.8
Arctic	0°-360°	60°-90°N	4.2	4.2	4.6	4.8	5.2
North extratropics <sup>2</sup>	0°-360°	20°-60°N	4.8	4.8	4.7	4.7	4.9
Tropical oceans <sup>2</sup>	0°-360°	20°S-20°N	5.6	5.6	5.5	5.5	5.5
South extratropics <sup>2</sup>	0°-360°	60°-20°S	6.8	6.8	6.8	6.8	6.8
Antarctic	0°-360°	90°-60°S	5.9	5.9	5.6	5.8	5.8

<sup>1</sup>Only values over land are considered for the calculation of pH

<sup>2</sup>Only values over oceans are considered for the calculation of pH